Heliyon 10 (2024) e30174

Contents lists available at ScienceDirect

Heliyon

journal homepage: www.cell.com/heliyon

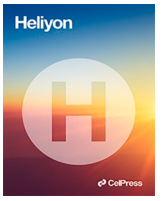

Research article

Optimal channel dynamic selection for Constructing lightweight Data EEG-based emotion recognition

Xiaodan Zhang [a,*], Kemeng Xu [a], Lu Zhang [a], Rui Zhao [a], Wei Wei [a], Yichong She [b]

[a] School of Electronics and Information, Xi'an Polytechnic University, Xi'an, Shaanxi, 710600, China
[b] School of Life Sciences, Xi Dian University, Xi'an, Shaanxi, 710126, China

ARTICLE INFO

Keywords:
emotion recognition
Lightweight data
Optimal channels
ACO–CNN–LSTM

ABSTRACT

At present, most methods to improve the accuracy of emotion recognition based on electroencephalogram (EEG) are achieved by means of increasing the number of channels and feature types. This is to use the big data to train the classification model but it also increases the code complexity and consumes a large amount of computer time. We propose a method of Ant Colony Optimization with Convolutional Neural Networks and Long Short-Term Memory (ACO–CNN–LSTM) which can attain the dynamic optimal channels for lightweight data. First, transform the time-domain EEG signal to the frequency domain by Fast Fourier Transform (FFT), and the Differential Entropy (DE) of the three frequency bands (α, β and γ) are extracted as the feature data; Then, based on the DE feature dataset, ACO is employed to plan the path where the electrodes are located in the brain map. The classification accuracy of CNN-LSTM is used as the objective function for path determination, and the electrodes on the optimal path are used as the optimal channels; Next, the initial learning rate and batchsize parameters are exactly matched the data characteristics, which can obtain the best initial learning rate and batchsize; Finally, the SJTU Emotion EEG Dataset (SEED) dataset is used for emotion recognition based on the ACO–CNN–LSTM. From the experimental results, it can be seen that: the average accuracy of three-classification (positive, neutral, negative) can achieve 96.59 %, which is based on the lightweight data by means of ACO–CNN–LSTM proposed in the paper. Meanwhile, the computer time consumed is reduced. The computational efficiency is increased by 15.85 % compared with the traditional CNN-LSTM method. The accuracy can achieve more than 90 % when the data volume is reduced to 50 %. In summary, the proposed method of ACO–CNN–LSTM in the paper can get higher efficiency and accuracy.

1. Introduction

The urgent demand for artificial intelligence in various domains has spurred the emergence of interdisciplinary approaches [1,2]. Specifically, there has been significant focus on utilizing computer technology and mathematical methods to process human biological signals [3,4]. EEG-based emotion recognition is one of the hot spots research topics that have received continuous attention [5–7]. EEG characterizes voltage fluctuations from the cerebral cortex and has been shown to reveal important information about the true

* Corresponding author.
E-mail addresses: zhangxiaodan@xpu.edu.cn (X. Zhang), xvkemeng@126.com (K. Xu), z001106z@163.com (L. Zhang), ruizhao@xpu.edu.cn (R. Zhao), weiwei@xpu.edu.cn (W. Wei), ycshe@stu.xidian.edu.cn (Y. She).

https://doi.org/10.1016/j.heliyon.2024.e30174
Received 17 July 2023; Received in revised form 12 April 2024; Accepted 22 April 2024
Available online 25 April 2024

emotional state of human [8–10]. EEG-based emotion recognition has been rapidly developed in the fields of artificial intelligence, medical care, and education [11–13].

Early EEG-based emotion recognition algorithms were mainly based on traditional machine learning methods, including support vector machines (SVM), K-nearest neighbors, random forests, naive Bayes, etc [14–16]. Yang F et al. [17]proposed an effective cross-subject sentiment recognition method that integrated significance testing, sequential backward selection and support vector machine (ST-SBSSVM). It ultimately achieved 89 % accuracy on the SEED dataset. Wagh K P et al. [18]used wavelet transform and extracted features such as Power Spectral density (PSD), Energy, Standard Deviation, and Variance, to classify the emotional states. Using three classifiers and the final decision tree had the highest accuracy of 71.52 %.

With the development of technology, deep learning techniques were also heavily applied to EEG signal emotion recognition [19–21]. Zhong P et al. [22] proposed a method based on regularized graph neural networks (RGNN) for emotion recognition of EEG, which accuracy was 94.24 % on the SEED dataset. Liu et al. [23] performed empirical mode decomposition and differential entropy feature extraction on the data, designed the optimal placement of electrodes. They finally fed the processed data into a two-dimensional CNN, which achieved the highest accuracy of 97.56 % on the SEED dataset. Yin et al. [24] calibrated and segmented the EEG signal and used the differential entropy feature as input to a deep learning model fusing model of graph convolutional neural networks and a long and short-term memory. The final average classification accuracies in arousal and valence were: 90.45 % and 90.60 %. Li et al. [25] designed a Bi-hemisphere domain adversarial neural network model (BiDANN) to reduce the possible domain differences between the source and target domains in the left and right hemispheres, which achieved an average accuracy of 92.38 %. Bao G et al. [26] proposed a data augmentation model of VAE-D2GAN, to generate an adversarial network model for emotion recognition on the SEED dataset with 92.5 % accuracy. Iyer A et al. [27] used differential entropy features of five frequency bands, combined with CNN and LSTM models, and finally achieved 97.16 % accuracy on the SEED dataset.

In addition, the scholars researched in the optimization of classification models [28–31]. Zg A et al. [32] optimized the CNN parameters and implemented sentiment recognition using an improved Particle Swarm Optimization (PSO). The experimental results showed that the average accuracy was 92.44 %, which had increased by 0.79 %. Lokesh, S. et al. [33]proposed Fractional Chimpanzee Optimization Algorithm (FrChOA) which combined the Chimpanzee Optimization Algorithm (COA) with fractional order calculus, and its classification accuracy was 88.48 % with 20 channels selected. Kannadasan K et al. [34] proposed a differential-evolution-based feature selection algorithm (DEFS) to obtain an optimal feature set for effective subject-independent for emotion recognition with SVM (DEFS-SVM). It got the classification accuracies of 73.60 % and 74.23 % to detect valence arousal and valence on the DEAP dataset, and they were higher than the Particle Swarm Optimization(PSO) feature selection algorithm by 9.55 % and 9.3 %, respectively.

In summary, most of the above studies used the data of all bands and channels. Although there was a selection of channels, the recognition accuracies were not well. In addition, more features were added beyond DE to improve classification accuracy. Although it can get higher classification accuracies, the more data needed to be processed which consumed more time and reduced the computational efficiency. In this paper, an ACO–CNN–LSTM algorithm was proposed with the goal of efficient and high-precision recognition, which can achieve higher-precision classification accuracy with a lightweight data of a single feature.

2. Method

In this paper, FFT was used to transform the EEG signal from time domain to frequency domain, so as to obtain five frequency bands: δ (<4Hz), θ (4–7Hz), α (8–13Hz), β (14–30Hz), γ (>30Hz), and the data of three frequency bands(α, β and γ) were used highly associated with emotion [35]. For feature extraction, only DE was used as the feature.

2.1. Differential entropy (DE)

DE is an extension of Shannon's information entropy on continuous variables, which can reflect the vigilance changes of continuous variables. EEG is the high-dimensional nonlinear data, and DE can provide dynamic and time-series information of EEG [36,37]. Meanwhile, DE has better robustness to noise and signal variation for EEG signals. Due to EEG's susceptibility to interference and information mutation, using DE as the feature can better cope with the above problems [38–40]. It can quantify some uncertainty in the probability distribution of continuous random variables, it is often used to analyze the complexity and uncertainty of EEG signals. DE is defined in Eq. (1):

$$DE = -\int_a^b p(x)\log(p(x))dx \tag{1}$$

in which, $p(x)$ is the probability density function of the information, [a,b] is the integral interval.

If the signal obeys or approximately obeys a Gaussian distribution $N(\mu,\sigma^2)$, its DE can be approximated to obtain a more easily calculated formula [41]. For the pre-processed EEG signals in each frequency band, they all approximately obey the Gaussian distribution. Thus DE of the i^{th} frequency band is shown as Eq. (2).

$$DE(i) = -\int_a^b \frac{1}{\sqrt{2\pi\sigma_i^2}} e^{-\frac{(x-\mu)^2}{2\sigma_i^2}} \log\left(\frac{1}{\sqrt{2\pi\sigma_i^2}} e^{-\frac{(x-\mu)^2}{2\sigma_i^2}}\right) dx = \frac{1}{2}\log\left(2\pi e\sigma_i^2\right) \tag{2}$$

in which, σ_i^2 denotes the signal variance of the i^{th} frequency band.

2.2. Convolutional neural network and Long Short-term memory (CNN-LSTM)

2.2.1. Convolutional neural network (CNN)

CNN is a feedforward neural networks that include convolutional computation with the deep structure. CNN is initially widely used in the image field, and with the development of deep learning, more and more scholars are applying CNNs to the other fields such as EEG signal emotion recognition [42]. CNN is consisted of convolutional layer, activation function, pooling layer, fully connected layer and output layer. Fig. 1 shows the structure of the classical CNN model.

2.2.2. Long Short-term memory (LSTM)

LSTM is a temporal recurrent memory network, which is one of the best known recurrent neural networks, and widely used in natural language processing, time series analysis and other serial data modeling tasks [43]. The memory unit in LSTM can be viewed as a state vector that retains important information in the input sequence and updates over time. LSTM also includes three gating units: forget gate, input gate and output gate. These gates can read, write, and clear memory cells based on the input sequence and the state from the previous moment. LSTM is highly capable of managing long-term dependencies. Fig. 2 shows the structure of the classical LSTM model.

2.2.3. CNN-LSTM

LSTM is utilized with CNN (CNN-LSTM), which can overcome the problem of CNN ignoring time information because EEG signal is a kind of time-series data [43]. Based on literature review, it has been observed that most network models consist of an input layer, convolutional layers, pooling layers, LSTM layers, dropout layers, fully connected layers, and a classification layer. For the number of CNN and LSTM layers, an overfitting model with 10 CNN layers and 4 LSTM layers was initially developed. Then the number of layers were reduced gradually to mitigate overfitting. Finally, a model with 4 CNN layers and 3 LSTM layers was chosen. Among them, each CNN hidden layer consists of one convolutional layer, one normalization layer and one maximum pooling layer. The model structure of CNN-LSTM is shown in Fig. 3.

For the convolutional layers, the Relu function is used in the model as the activation function for all four layers, and the convolutional kernel size is 3×1. The number of convolutional kernels in the first layer is 16, and the step size is 2×1, while the number of convolutional kernels in the next three layers is 32, and the step size is 1×1; For the pooling layer, this paper uses maximum pooling with a pool size of 2×1 and a step size of 1×1; The LSTM has three hidden layers and the number of hidden layers in each layer is 200, 100, 50 respectively. The output of the fully connected layer is three; For the dropout layer, the parameter is set to 0.2, which means that 20 % of the samples are randomly discarded in each training epoch, which serves to prevent over fitting. The set parameters of the CNN-LSTM are shown in Table 1.

2.3. ACO–CNN–LSTM

ACO is a heuristic path optimization algorithm based on the foraging behavior of ants in nature. The ants can release a special secretion (pheromone) on the path in search of food. Over time, the probability that later ants will choose that path is proportional to the concentration of pheromone on the path [44–46]. In the field of emotion recognition based on the EEG, there is a close relationship between emotion and channel, because the emotional states cause neural activity in different areas of the brain, and the electrical signals of these neural activities are acquired by the electrodes. The electrode positions are the fixed points of the paths, and ACO–CNN–LSTM can search the optimal channel of the optimal path and obtain the classification results. Table 2 shows the pseudo code of searching optimal channels by ACO–CNN–LSTM.

ACO–CNN–LSTM takes the classification accuracy of the CNN-LSTM as the objective function, continuously calculates the probability transfer matrix for each ant, and updates the pheromone to obtain the subset of historical optimal channels with the highest classification accuracy. Fig. 4 shows the recognition process of ACO–CNN–LSTM.

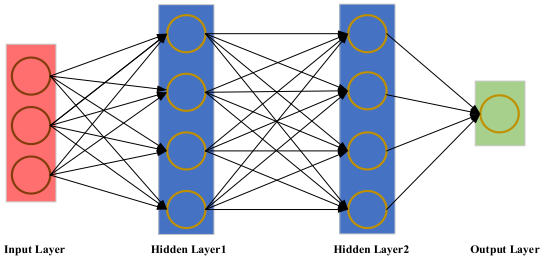

Fig. 1. Classical CNN model structure.

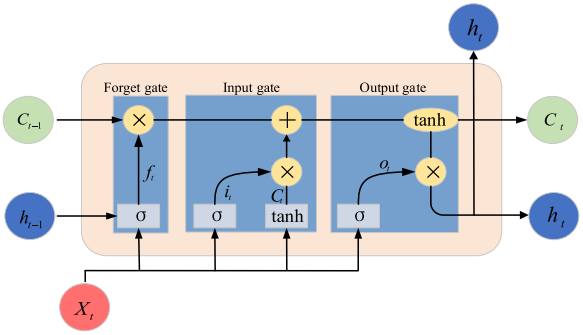

Fig. 2. Classical LSTM model structure diagram.

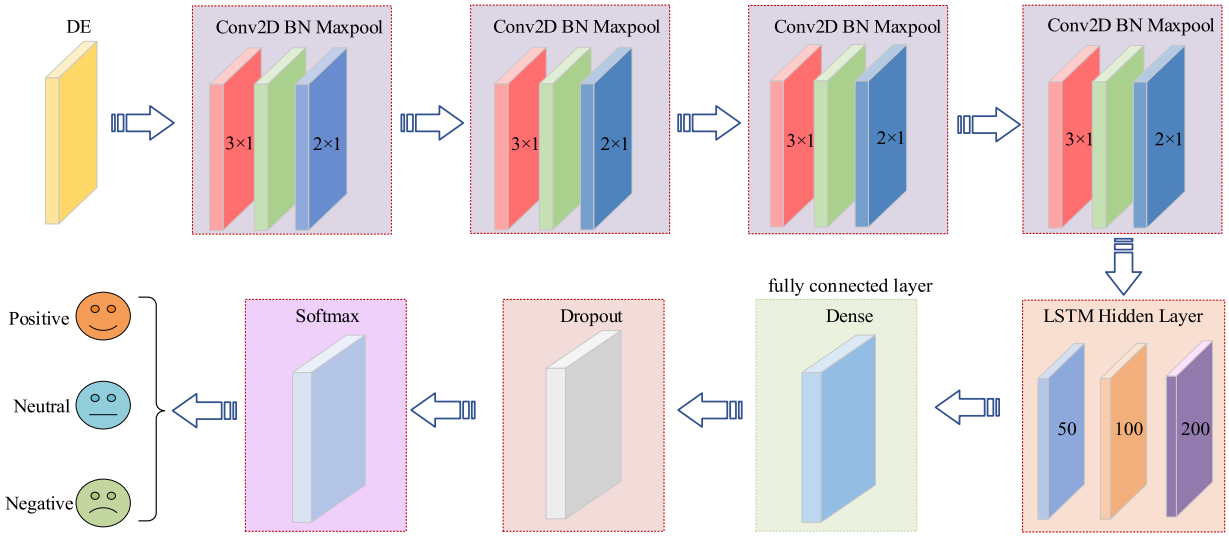

Fig. 3. CNN-LSTM structure diagram.

Table 1
The parameters of CNN-LSTM.

Layer Type	Filter size	Filter number	Stride size	Activation Function	Padding
Conv 1	3 × 1	16	2 × 1	RELU	Same
Pool 1	2 × 1	–	1 × 1	–	–
Conv 2	3 × 1	32	1 × 1	RELU	Same
Pool 2	2 × 1	–	1 × 1	–	–
Conv 3	3 × 1	32	1 × 1	RELU	Same
Pool 3	2 × 1	–	1 × 1	–	–
Conv 4	3 × 1	32	1 × 1	RELU	Same
Pool 4	2 × 1	–	1 × 1	–	–
LSTM 1	–	200	–	–	–
LSTM 2	–	100	–	–	–
LSTM 3	–	50	–	–	–
Dense	–	3	–	–	–
Dropout	0.2	–	–	–	–
Softmax	–	–	–	–	–

2.4. Dataset

SEED dataset was employed for emotion recognition in this paper. The dataset consisted of 15 subjects (7 males and 8 females), which the average age was 23.27 and 15 experiments of each subject. Fifteen Chinese film clips (positive, neutral and negative emotions) were chosen from the pool of materials as stimuli used in the experiments and the experiments were repeated three times at

Table 2
Search optimal channels by ACO–CNN–LSTM.

Algorithm: ACO–CNN–LSTM
Input: D: All EEG Data G: Number of iterations m: Number of ants ch: Number of channels P0: Transfer probability constant Output: A subset of historical optimal channels with ch channels. 1: Set the initial subset of channels randomly 2: Initialize pheromone matrix ξ 3: while iter < G do 4: for i = 1 to m do 5: Calculate CNN-LSTM-baesd classification accuracy of the channels constructed by the i^{th} ant 6: Calculate the state transfer probability P of the i^{th} ant 7: if P ≤ P0 then 8: Selecting a new channel using roulette wheel algorithm 9: end if 10: end for 11: Select the channel with the highest classification accuracy in the iter to update the pheromone ξ 12: end while 13: Select the channels corresponding to the highest pheromone ξ as the best channels

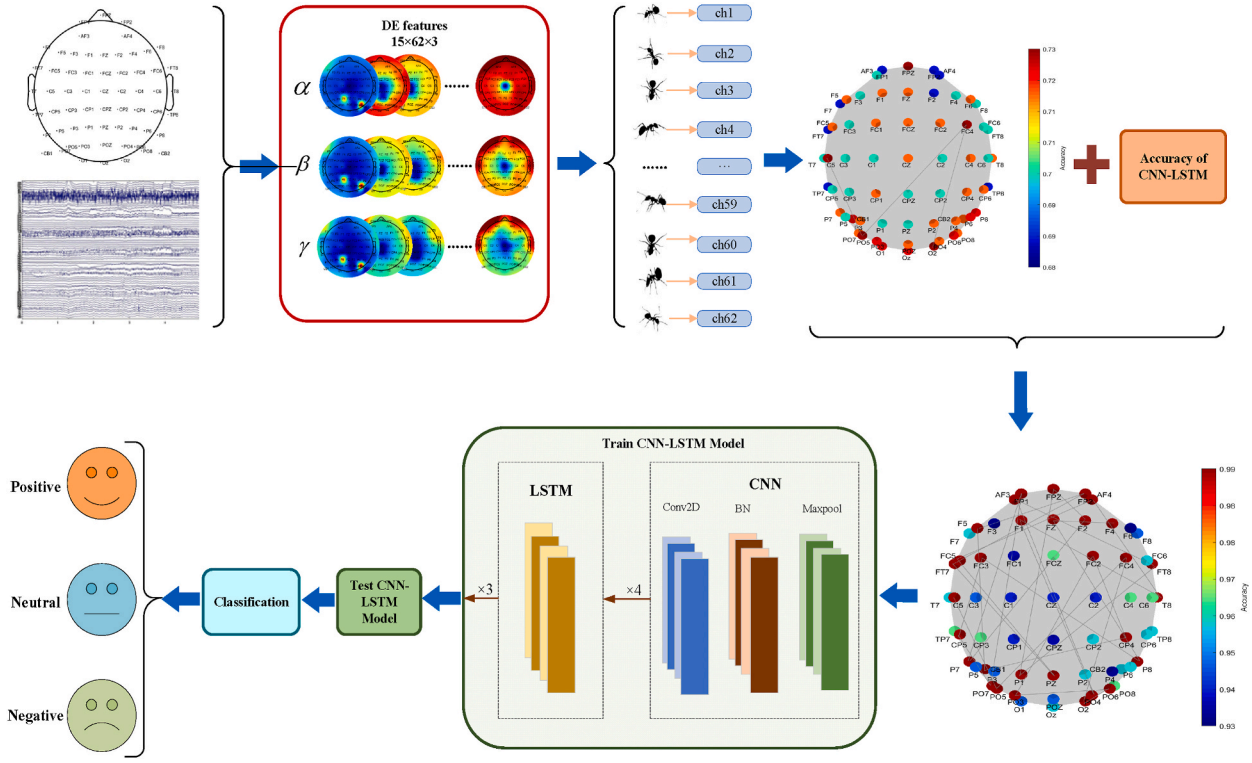

Fig. 4. The recognition process of ACO–CNN–LSTM.

sequential intervals of one week. The duration of each film clip is approximately 4 min. Each film clip is well edited to create coherent emotion eliciting and maximize emotional meanings. The details of the film clips used in the experiments were listed in Table 3. There were a total of 675 samples, each of which contains 62 channels. The ratio of training set to test set was 4:1, the data size of training set was 540 × 62 × 3 and the data size of test set was 135 × 62 × 3.

Table 3
The details of the film clips [47].

No.	Emotion label	film clips sources
1	negative	Tangshan Earthquake
2	negative	Back to 1942
3	positive	Lost in Thailand
4	positive	Flirting Scholar
5	positive	Just Another Pandora's Box
6	negative	World Heritage in China

3. Experimental results and analysis

3.1. Feature experiments and analysis

Using a single feature as the feature data for classification implied that the feature exhibits strong EEG emotion characteristics. Emotion classification experiments were conducted on seven features, as shown in Table 4. The classification results were shown in Fig. 5, which was to illustrate the reason for choosing DE as the single feature.

As can be seen from Fig. 5, the classification accuracy of each feature increased with the increase of the number of iterations. Among them, the recognition accuracy of the DE used in this paper was significantly higher than the others, and its accuracy rate can reach 100 % in the 60th iterations. It can be seen that DE can capture the nonlinear dynamic characteristics of EEG signals. Therefore, DE was selected as the feature data for EEG emotion recognition in this paper.

People has different psychological perceptions and emotional expression because of their different life trajectories, and there may be some significant differences in the performance of the same and different sex in response to the same stimulus. Figs. 6 and 7 showed DE head distribution of 15 subjects on the frequency bands of α、 β and γ, which stimulus were the same of positive. Fig. 6 showed DE head distribution of 7 male subjects and Fig. 7 showed DE head distribution of 8 female subjects.

From Figs. 6 and 7, it can be seen that the concentrated regions of the low DE were basically consistent both males and females, and the electrode regions of males are larger than females. But among the males, S01 and S06 showed specificity with high DE. The electrodes with high DE of S01 were located at PO6 and P1, and the electrodes with high DE of S06 were located at AF4 and P1. It indicated that the above two male subjects were different from the other subjects, and also indicated the individual differences because they showed different responses to the same stimulus. Among the females, S15 subject showed the individual differences. The high DE electrodes of S15 were located at FC5, PO3, AF4, F2, FC2 and P5. It indicated that S15 showed many differences to the others, stimuli, and this subject should be put into the training set to strengthen the generalization ability of the classification model.

Table 4
The seven features.

Feature	Expression	Explanation
Average (ave)	$ave = \frac{\sum_{i=1}^{N} x_i}{N}$ (3)	x_i and $x(t)$ represents the set of EEG signals corresponding to one of the channels after pre-processing.
Standard Deviation (std)	$std = \sqrt{\frac{\sum_{i=1}^{N}(x_i - ave)^2}{N}}$ (4)	σ_n^2 represents variance of the EEG signal. N is the sequence length of this EEG signal.
Hjorth	$Activity = \sigma_n^2 = \frac{1}{N}\sum_{i=1}^{N}[x_i - ave]^2$ (5)	
	$Mobility = \sqrt{\frac{Activity\left(\frac{d(x(t))}{dt}\right)}{Activity(x(t))}}$ (6)	
	$Complexity = \frac{Mobility\left(\frac{d(x(t))}{dt}\right)}{Mobility(x(t))}$ (7)	
DE	$DE(i) = \frac{1}{2}\log(2\pi e\sigma_i^2)$ (8)	$\sigma_i{}^2$ denotes the signal variance of the i^{th} frequency band.
Power Spectral Density (PSD)	$PSD = \frac{1}{2\pi N}\left\|\sum_{n=0}^{N-1} x(n)e^{-jon}\right\|^2$ (9)	N is the sequence length of the segment of discrete EEG signals. $x(n)$ represents the set of EEG signals corresponding to one of the channels after pre-processing.
Fractal dimension (FD)	$FD = \frac{\log(L)}{\log(d)} = \frac{\log\left(\frac{L}{a}\right)}{\log\left(\frac{d}{a}\right)} = \frac{\log(N)}{\log(N) + \log\left(\frac{d}{L}\right)}$ (10)	N is the number of time samples in the EEG epoch. d is the distance between the two consecutive points (curve diameter) and L denotes the curve. length.
Mean and Standard Deviation of wavelet coefficients (MS-DWT)	$w_f(a,b) = \frac{1}{\sqrt{a}}\int_R f(t)\overline{\varphi\left(\frac{t-b}{a}\right)}dt (a > 0)$ (11)	$\varphi(t)$ is called wavelet function or wavelet mother function. a is the scale factor and b is the translation factor.

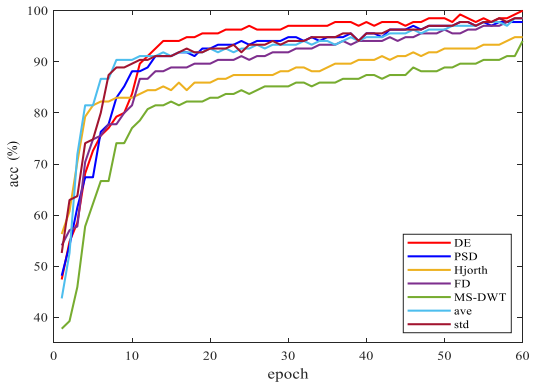

Fig. 5. Single feature classification results.

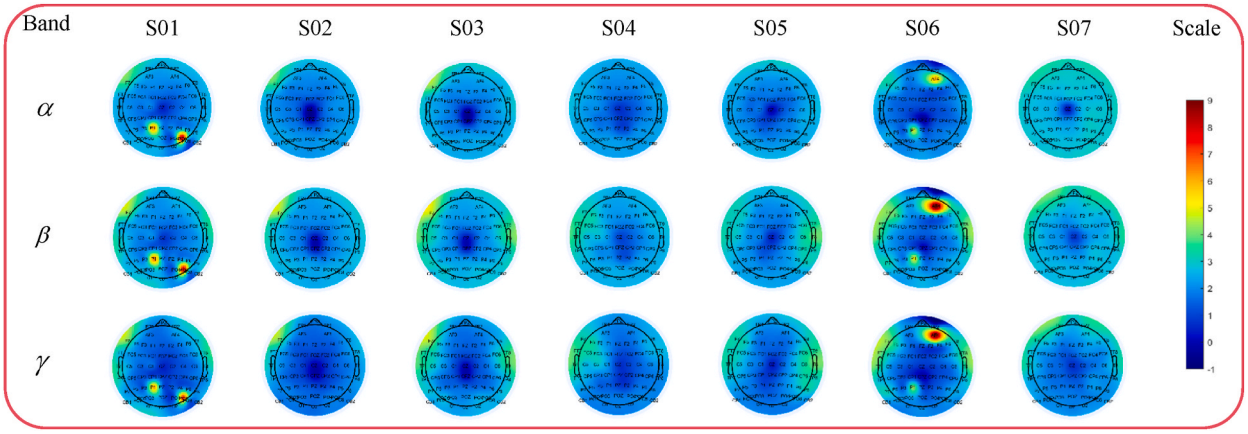

Fig. 6. DE head distribution of 7 male subjects.

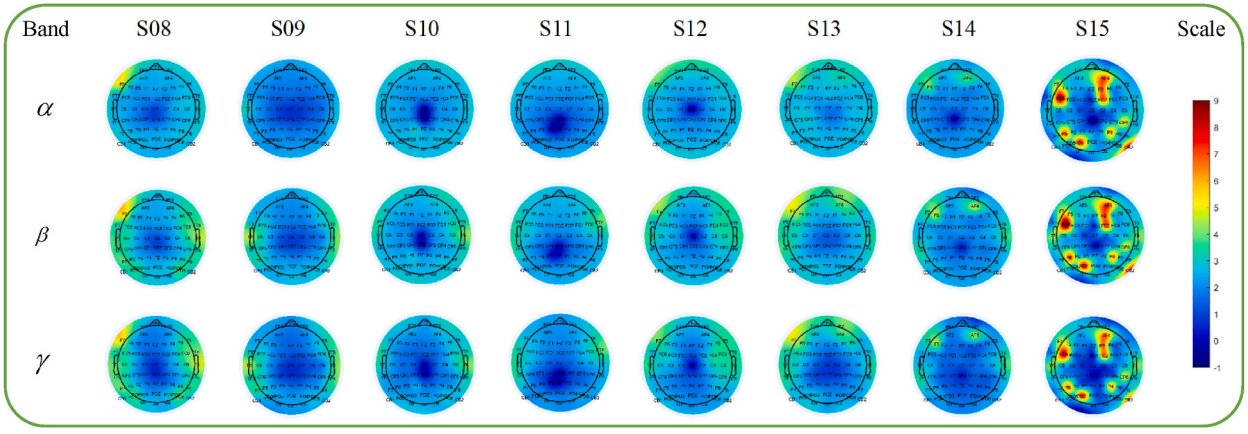

Fig. 7. DE head distribution of 8 female subjects.

3.2. Initial learning rate and batchsize analysis

The ratio of training set to test set was 4:1, the data size of training set was $540 \times 62 \times 3$ and the data size of test set was $135 \times 62 \times 3$. The initial learning rate and batchsize had a great impact on the classification of CNN-LSTM model. The learning rate had a hold on the step size of each parameter update, and the batchsize had a hold on the number of samples used in each iteration. It is necessary to choose the appropriate initial learning rate and batchsize while ensuring the stability and generalization ability of the model.

(1) Initial learning rate analysis

The initial learning rate (η) is one of the key hyper-parameters for optimizing algorithm. A smaller initial learning rate will make the more stable of training, but more time to converge and may even trapped in a local optimum solution in the early training; A larger initial learning rate may cause to oscillate or fail to converge in the early training. Based on the value interval of initial learning rate [0.0001,0.01] [48], five initial learning rates ($\eta = e-2$, $\eta = 5e-3$, $\eta = e-3$, $\eta = 5e-4$ and $\eta = e-4$) were tested in this paper for better performance, and the accuracies of the training and test sets were shown in Fig. 8.

In Fig. 8 it can be seen that the accuracy rates of the training and test sets were both close to 100 % with 50 iterations, and the accuracy rates of the training was slightly higher than test. The accuracy rate of the training and test sets both reached the highest when $\eta = 5e-4$ (red line). In Fig. 8(a), the accuracy rate was the lowest when $\eta = e-2$, and after 45 iterations, they all tended to stabilize and were relatively close, but it can be seen clearly that the red line was the highest in the enlarged image of details. In Fig. 8(b), the accuracy rate was the lowest when $\eta = e-2$, which was the same as training set. When $\eta = e-2$, $\eta = 5e-3$, $\eta = e-3$,which were larger than $\eta = 5e-4$, they would lead to the insufficient learning of the model and failed to converge or oscillating across the optimal solution, and resulted in a lower accuracy rate; And when $\eta = e-4$,which is smaller than $\eta = 5e-4$, it trained and converged slowly, possibly converging at local extremes.

Therefore, $\eta = 5e-4$ was employed as the initial learning rate, using the Adam as the gradient descent method. As the number of iterations increased, the learning rate was gradually reduced in the process of approaching the optimal solution, and the reduction rate was 10 % of the previous rate for every 10 epochs of training.

(2) Batchsize analysis

The batchsize has a hold on the number of samples in each training round. If the batchsize is set too small, the randomness of the model is too high to learn the overall pattern of the dataset; If the batchsize is set too large, it may consume too much memory and computational resources, which is not conducive to convergence to the global optimal solution. The classification accuracy of the training and test sets with different batchsize were shown in Table 5.

It can be seen from Table 1 that the batchsize didn't have much effect on the training set, the accuracy could reach more than 99 %. However, in the test set, the influence of the batchsize on the classification accuracy was obviously. The classification accuracy of the test set showed that the mean highest accuracy (96.99 %) appeared while batchsize = 16 with 60 epochs. It was because the smaller batchsize for model may lead to sticking a local optimal solution and overfitting; And the larger batchsize for model led to, decreasing the number of iterations and unable to converge. Therefore, batchsize = 16 was chosen for ACO–CNN–LSTM in the paper.

3.3. Optimal channels dynamically selection

ACO–CNN–LSTM was used on optimal channel selection of SEED dataset which contained 62 channels. In the finding path using ACO–CNN–LSTM, it was started by 3 channels randomly which was shown in the first one in Fig. 9, and the training set and the test set were randomly too, and ACO–CNN–LSTM can dynamically select the optimal channels for those, the method can select the optimal channels for different training set and test set, so the optimal channels were dynamic. 30 times were experimented for different training set and test set, and the highest accuracy and efficiency can be achieved with 31 optimal channels.

The process of optimal channels selection was shown in Fig. 9, and the line in it indicated the optimal channel path passed. As can be seen from Fig. 8, the accuracy kept improving as the number of channels increasing, and the accuracy was highest when the number of channels was 31, and the red color of the points of 32 channels were obviously lighter than 31 channels, which meant that the accuracy decreased; the red color of the points of 33 channels and 34 channels were almost the same as 31 channels, but the average accuracy of them were lower than 31channels. Table 4 showed the accuracy and computer time using ACO–CNN–LSTM by selecting

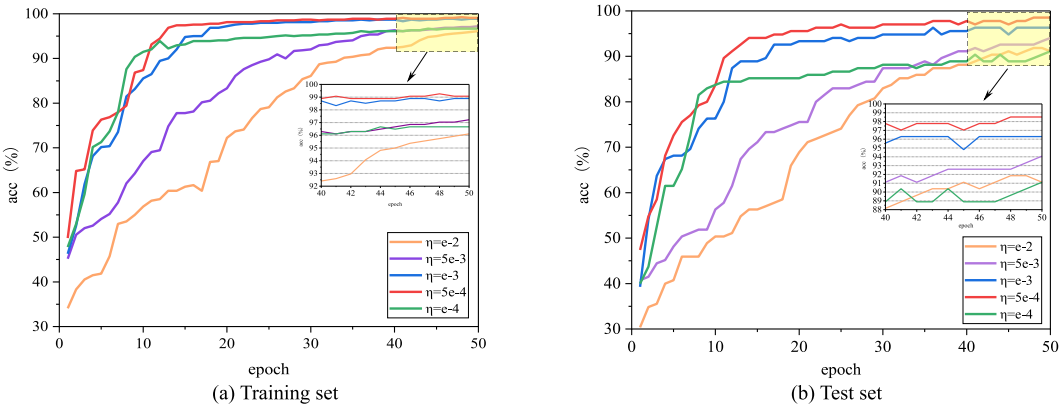

Fig. 8. The impact of learning rate η on accuracy.

Table 5
The mean classification accuracy of different batchsize with different epoch.

Batchsize / Dataset Epoch	4(%)		8(%)		16(%)		32(%)	
	Training	Test	Training	Test	Training	Test	Training	Test
10	88.77	82.72	92.99	88.79	93.59	88.54	93.25	87.60
20	96.98	94.22	97.09	93.83	96.72	94.67	95.73	94.52
30	98.99	94.57	98.63	94.72	99.14	94.97	99.14	94.86
40	99.15	95.51	99.17	95.99	99.25	96.45	99.19	95.60
50	99.22	95.85	99.21	96.15	99.28	96.74	99.20	96.19
60	99.22	95.95	99.23	96.59	**99.44**	**96.99**	99.31	96.25
Average	97.06	93.14	97.72	94.35	**97.90**	**94.73**	97.64	94.17

16, 31, 48 and 62 channels, respectively.

As can be seen from Table 6, the time cost increased as the number of channels increases. When the number of channels was 31, the average accuracy of the training and test sets were 99.44 % and 96.99 %, both higher than the 16, 48 and 62 channels, but in only 54.15s, there was 15.85 % improvement in computational efficiency. The 31 optimal channels were C5, PO5, FC4, O2, PO6, PO3, FC2, CP4 CB1, F5, FP2, FT7, PZ, FC5, AF4, T8, F1, PO4, AF3, FT8, P1, FPZ, F2, P7, FP1, PO7, CP5, FC3, P8, FZ, F4, they were shown in Fig. 10, and the red points were the 31 optimal channels for this time. And the next time may not be these 31 optimal channels, ACO–CNN–LSTM could dynamically select the optimal channel based on different inputs and the initial subset of channels. Based on the experiments, using 31 channels can achieve the better accuracy and less computer time.

3.4. Experimental results and analysis of ACO–CNN–LSTM

ACO–CNN–LSTM was employed on SEED dataset, which training set: test set = 4:1. Fig. 11 showed the variation curves of 3-classification accuracy, recall, F1 score and AUC of the area under the ROC curve for 60 iterations. As seen from the curves in Fig. 10, each evaluation parameter in both the training and test sets increased with the number of iterations, and after 40 epochs the rise was slow, the accuracy of the training set stabilized and remained around 99 %, while the accuracy of the test set was rising with small fluctuations. Until 60 epochs, the test set's average classification accuracy can reach up to 96.99 %, the recall can reach 99.35 %, the F1 score can reach 99.31 %, and the AUC can reach 98.54 %.

Fig. 12 showed the confusion matrix for the test set with three classifications (positive, neutral and negative) based on the ACO–CNN–LSTM. As seen from Fig. 10, the positive and neutral states were correctly predicted, and only one error was found in the negative state out of 135 test samples, and the classification accuracy reached 99.26 %.

To analyze the misjudgment subjects, 45 samples were extracted from three experiments of each subject for misjudgment analysis. Fig. 13 showed the Sankey diagram of the flow of classification results for the above 45 samples.

In Fig. 13, the left number was the subject number, and the middle number was the experiment number corresponding to each subject. For example, the 7th subject number was 7, and its 2nd experiment number was E072. The three classification (positive, neutral, and negative) was shown on the right. From Fig. 13, it can be seen that E012 was misclassified as negative emotion, which was originally neutral emotion. E012 was the 2nd experiment of the 1st male subject. He had already shown his differences in the 1st experiment which can been seen from Fig. 5. To provide a more detailed analysis of DE features for misclassified, the DE values of 15 subjects in the 2nd experiment of three bands (α, β and γ) were shown in Fig. 14.

From Fig. 14, it can be seen that the DE values of S01 and S15 exhibited significant differences from other subjects, which DE values were much bigger than the others. However, the classification of S15 was correct, so we analyzed the training set. It found that the S15 subject had been in the training set for training, so S15 was classified correctly, and S01 was outside the training set, so S01was misclassified. Then the S01 was put to training set and obtained classification accuracy of 100 %.

4. Discussions

ACO–CNN–LSTM for EEG signal emotion recognition proposed in this paper could select the optimal channels, make the data lighter, improve the algorithm accuracy and efficiency, and obtain better results through the experiments in this paper. In the following, the effectiveness of ACO–CNN–LSTM proposed was discussed in terms of both comparison with traditional CNN-LSTM and existing references.

4.1. Comparison with traditional CNN-LSTM

The box plots of the classification accuracy of the two methods obtained using ACO–CNN–LSTM and CNN-LSTM for emotion classification based on SEED dataset were shown in Fig. 15.

From Fig. 15(a), it can be seen that the median classification accuracy of the training set based on the CNN-LSTM was 99.07 %. Meanwhile, the average was 99.10 %, and the standard deviation was 0.4512; The median classification accuracy of the test set was 96.67 %. Meanwhile, the average was 96.37 % and the standard deviation was 2.3533. From Fig. 15(b), it can be seen that the median accuracy of the training set based on the ACO–CNN–LSTM method was 99.44 %. Meanwhile, the average was 99.32 % and the standard

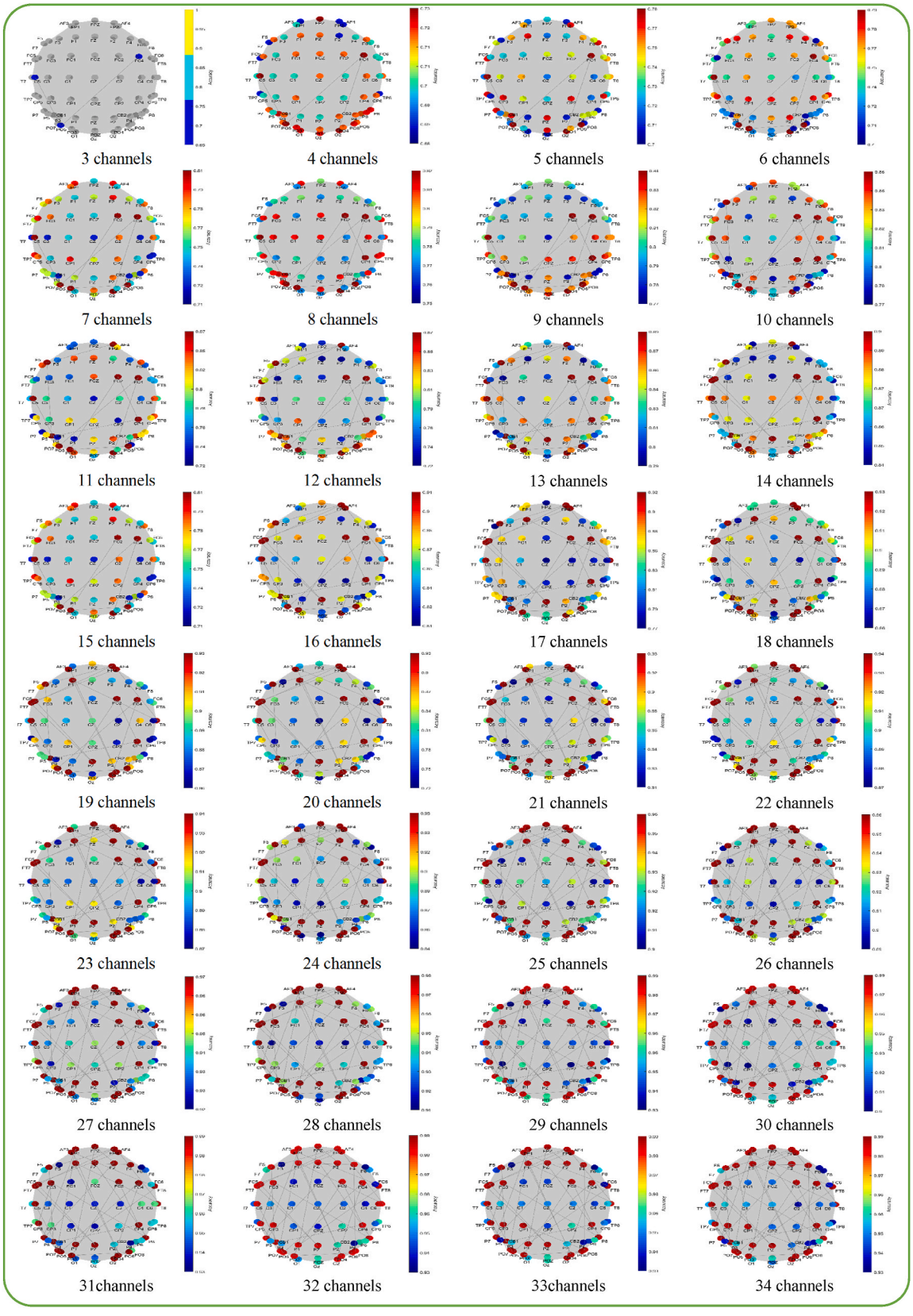

Fig. 9. Optimal channel selection path base on ACO–CNN–LSTM.

Table 6
Results of optimization of channels.

Channel number Dataset and time cost	16 channels	31 channels	48 channels	62 channels
Training set(%)	98.49	**99.44**	99.22	99.08
Test set(%)	92.32	**96.99**	96.47	96.37
Time cost$_{(s)}$	48.75	**54.15**	59.54	64.35

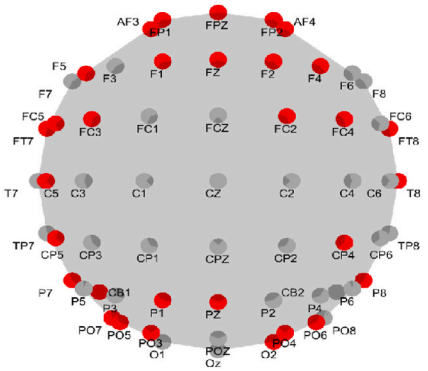

Fig. 10. 31 optimal channels.

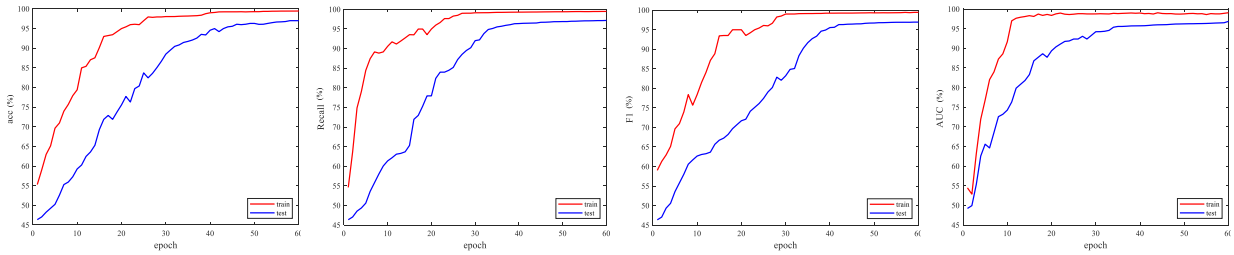

(a) accuracy (b) recall (c) F1 score (d) AUC

Fig. 11. Four-class evaluation parameter curves based on ACO–CNN–LSTM.

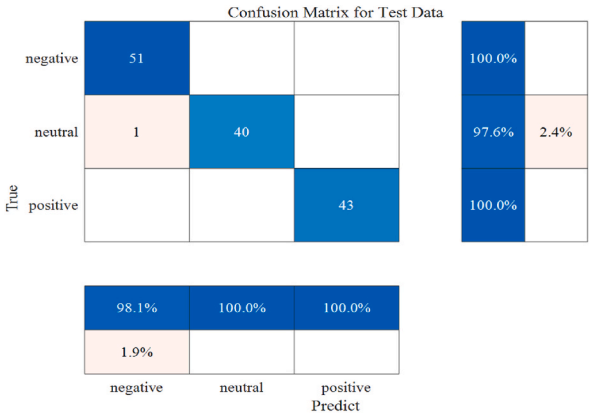

Fig. 12. Confusion matrix for test set.

deviation was 0.3346; The median classification accuracy of the test set was 97.04 %. Meanwhile, the average was 96.99 % and the standard deviation was 1.5554. From the comparison of the boxes in Fig. 15(a) and (b), it can be observed that the performance on the training set was not significantly improved after incorporating the ACO algorithm. However, on the test set, there was a noticeable enhancement in both recognition accuracy and its stability after integrating the ACO algorithm.

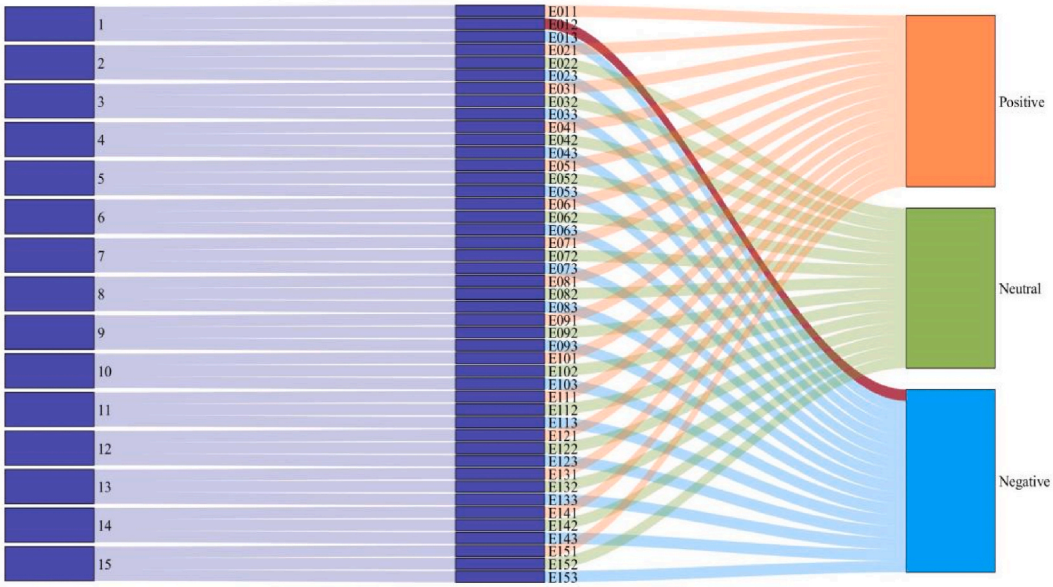

Fig. 13. Sankey of classification results for 45 samples.

The comparison of the classification accuracy was shown in Fig. 16, which showed that the accuracy of the training set was almost based on CNN-LSTM and ACO–CNN–LSTM, but the average accuracy of the test set was improved.

Fig. 16 also showed that ACO–CNN–LSTM was able to select the effective optimal channels and eliminate the channels that have little impact on classification or play a negative role. On the other hand, as can be seen from Fig. 15, the positive emotion recognition accuracies of ACO–CNN–LSTM and CNN-LSTM were both better than the other emotions, which may be because the EEG of positive emotion was more obvious in terms of emotion expression and stronger signal intensity. From Fig. 16(a), it can be seen that in the test set, the average classification accuracy of CNN-LSTM for positive emotions reached 98.14 %, neutral emotions reached 95.8 %, and negative emotions reached 93.81 %; As can be seen in Fig. 16(b), in the test set, the average classification accuracy of ACO–CNN–LSTM also reached 98.48 % for positive emotions, 95.8 % for neutral emotions, and 95.65 % for negative emotions. The comparison showed that the recognition accuracy for all three emotions on the test set had improved after integrating the ACO algorithm, especially for negative emotion. It illustrated the effectiveness of the ACO–CNN–LSTM proposed in this paper.

4.2. Data segmentation

Data segmentation can expand the sample size and achieve data augmentation. According to Ref. [26], Bao G and colleagues divided the data into non-overlapping 1-s segments, with each segment treated as a sample. To further investigate the algorithm proposed in our paper and improve recognition accuracy, data segmentation experiments were conducted. The principle of data segmentation experiments is illustrated in Fig. 17.

From Fig. 17, in the data segmentation experiments of our paper, 20 % of each segment's samples were used as new samples, with a 50 % overlap between consecutive new samples. By this way, the total sample size for the experiment can be increased tenfold. Meanwhile, the same segmentation method for emotion recognition was also used as Bao G et al. The experimental results were shown in Table 7.

As shown in Table 7, when using the same segmentation approach as reference [26], the classification accuracy in our study was higher than it. It evidently showed that our data segmentation approach had higher accuracy, recall, F1 score, and AUC compared to the results without data segmentation. However, the time cost is significantly higher of the segmented data, showing an increase of 834.55 % compared to the non-segmented data. Analyzing the reasons, data segmentation aimed to improve recognition rates by increasing the sample size entering the model. However, the increase in the number of samples also lead to a larger time cost. It is not applicable in situations with high real-time requirements.

4.3. Ablation study

To further validate the effectiveness of the module proposed in this paper, ablation experiments for ACO, CNN, LSTM, and ACO–CNN–LSTM were conducted each for 30 epochs. The experimental results were shown in Table 8.

From the experimental results in Table 8, compared to the algorithm proposed in this paper, when not using the ACO for channel optimization, the average accuracy was 96.37 %. It resulted in a decrease of 0.62 % in accuracy and an increase in runtime by 10.2 s. However, when the network structure was altered, whether using only CNN or only LSTM, the recognition accuracy was significantly

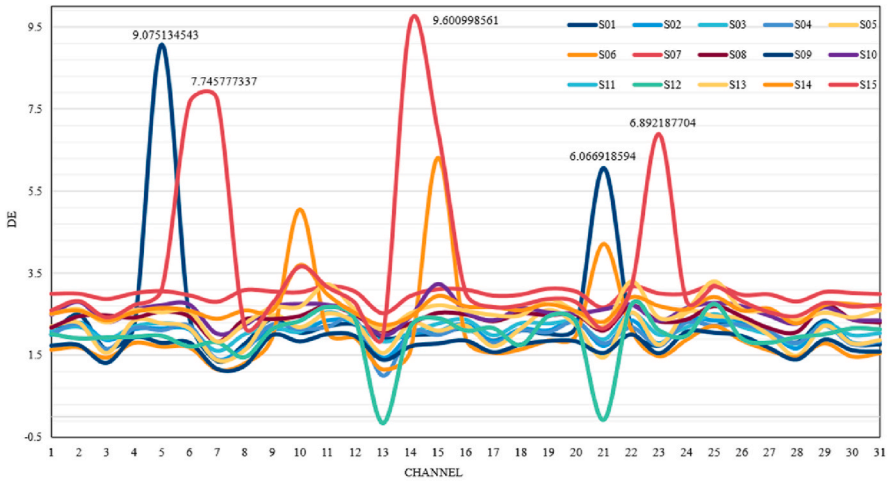

(a) The DE values of 15 subjects in the 2nd experiment of α band

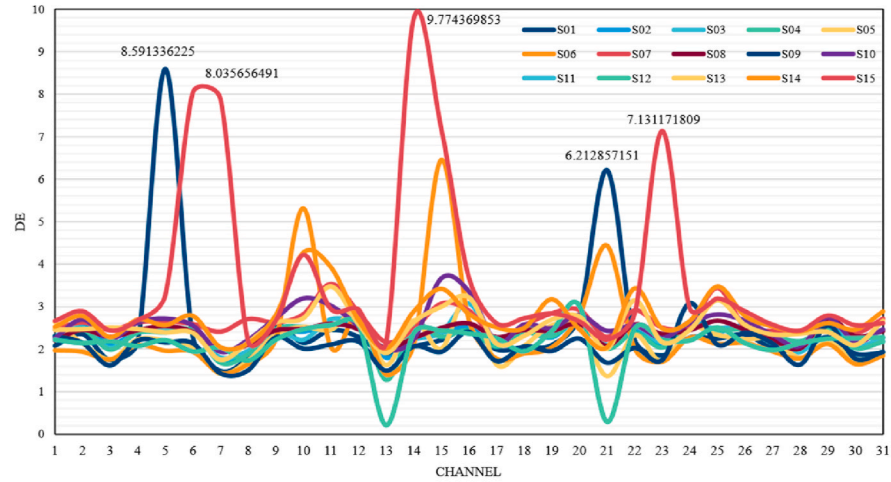

(b) The DE values of 15 subjects in the 2nd experiment of β band

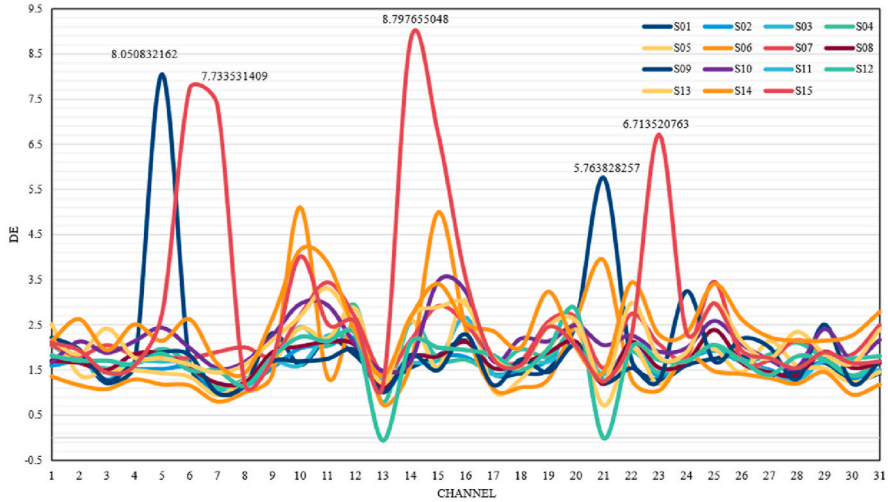

(c) The DE's values of 15 subjects in the 2nd experiment of γ band

Fig. 14. The DE values of 15 subjects in the 2nd experiment of three bands (α, β and γ).

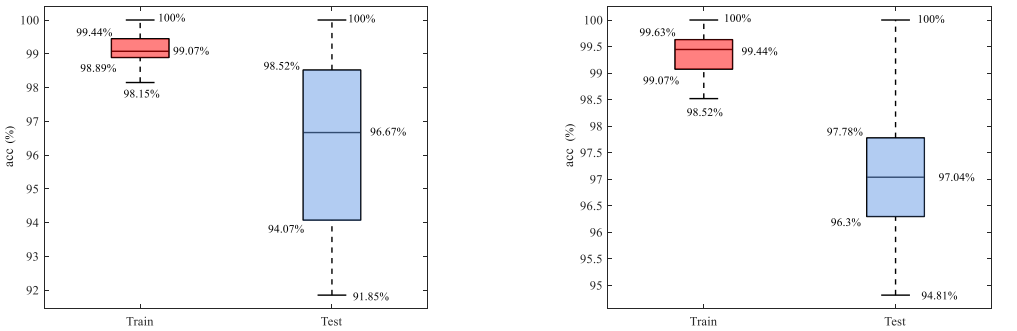

(a) CNN-LSTM accuracy box plot (b) ACO-CNN-LSTM accuracy box plot

Fig. 15. The comparison of accuracy box plots between CNN-LSTM and ACO–CNN–LSTM.

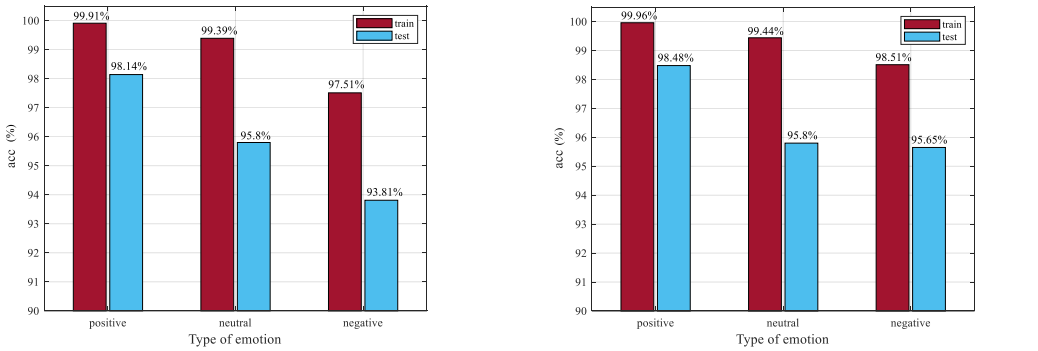

(a) CNN-LSTM emotion classification accuracy (b) ACO-CNN-LSTM emotion classification accuracy

Fig. 16. The comparison of three classification accuracies between CNN-LSTM and ACO–CNN–LSTM.

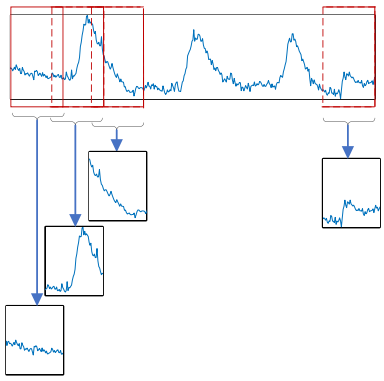

Fig. 17. The principle of data segmentation.

Table 7
Results of Data segmentation.

Item Data segmentation	Acc(%)	Recall(%)	F1 score(%)	AUC(%)	Time cost (s)
Reference [26]	92.5	–	–	–	–
Without data segmentation	96.99 ± 3.35	96.91 ± 1.61	96.86 ± 1.54	96.52 ± 2.01	54.15
Same data segmentation approach as Reference [26]	98.79 ± 0.10	98.79 ± 0.13	98.79 ± 0.11	98.89 ± 0.09	12932.54
Ours data segmentation approach	99.72 ± 0.19	99.62 ± 0.14	99.73 ± 0.23	99.74 ± 0.19	506.06

Table 8
Ablation experiments.

Item	Acc(%)	Recall(%)	F1 score(%)	AUC(%)	Time cost (s)
-ACO	96.37 ± 2.35	95.88 ± 2.09	96.17 ± 2.14	94.17 ± 3.50	64.35
-CNN	75.23 ± 4.5	75.1 ± 4.24	74.86 ± 4.24	66.85 ± 5.21	37.54
-LSTM	92.27 ± 3.76	92.36 ± 3.67	92.25 ± 3.68	90.79 ± 4.95	48.88
ACO–CNN–LSTM	96.99 ± 3.35	96.91 ± 1.61	96.86 ± 1.54	96.52 ± 2.01	54.15

lower than the recognition accuracy achieved by the CNN-LSTM model. Thus, it could be observed that all the modules implemented in our study were indispensable. The ACO algorithm not only reduced the processing time but also eliminated channels with lower relevance to emotions, thereby improving recognition accuracy. Although the time cost decreased when not using CNN or LSTM individually, the accuracy also dropped. The optimal performance was achieved only when both the CNN and LSTM modules were used simultaneously.

4.4. Comparison with existing references

ACO–CNN–LSTM proposed in this paper was compared with the existing references, and the results of the comparison were shown in Table 9. As shown in Table 9, when both extracted DE as feature data for classification, the average accuracy of emotion classification of the proposed ACO–CNN–LSTM method in this paper was higher than references [22,26,49,52,53]; When multiple features were used as classification data, the average accuracy of emotion classification by ACO–CNN–LSTM was still higher than references [18,54,55]. In terms of channels, the proposed ACO–CNN–LSTM was advanced in channel selection, and obtained the effective channels and the higher classification accuracy.

5. Conclusions and future work

The research has demonstrated that there was a close relationship between emotions and channels. ACO–CNN–LSTM proposed in the paper can dynamically select the optimal channels based on inputs and the initial subset of channels, which were high correlation with emotion. It can also reduce the data volume by 50 %, only using DE as the feature for recognition. In addition, the layers, initial learning rate and batchsize were designed of CNN-LSTM. The results showed that ACO–CNN–LSTM proposed in this paper used half of the data and obtained the higher accuracy to use all the data. ACO–CNN–LSTM was good in terms of accuracy and efficiency of lightweight data emotion recognition.

It is worth noting that ACO–CNN–LSTM proposed had been proven to be better for emotion recognition based on SEED dataset, it demonstrated higher classification accuracy and efficiency. So far, no scholars have used ACO optimized CNN-LSTM to apply in the field of channel optimization for EEG-based emotional recognition, and it is a dynamic selection process which can suitable for different input data and fields.

Our study also has some limitations. Research was only conducted on the SEED dataset. Due to different emotional reactions for the same stimulus among different ethnicities, gender, age, mentality and so on, and the subjects of SEED dataset are all Chinese, there may be limitations in generalizing the findings to populations in Europe, America, Africa, and other regions. In the future, large-scale datasets could be created. In addition, techniques such as transfer learning could be utilized to create an integrated framework for emotion recognition, aiming to enhance generalization capabilities.

Informed Consent Statement

The data used in this research is SEED dataset which is the public dataset.

Table 9
Comparison with the existing references.

References (Year)	Model	Feature	Number of channels	Average acc(%)
Song T [49] (2018)	DGCNN	DE	62	90.40
Wang, Z. M [50]. (2019)	P-GCNN	RASM	62	84.35
Zhong P [22] (2020)	RGNN	DE	62	94.24
Hwang S [51] (2020)	CNN	TP-DE	62	90.41
Rahman M A [54] (2020)	ANN	MaxNorm,L2Norm, Fractional Dimension.etc	62	86.57
Bao G [26] (2021)	GAN	DE	62	92.50
Li Y [25] (2021)	BiDANN-S	DE	62	92.38
Wagh K P [18] (2022)	RF	PSD, Energy, Standard Deviation, and Variance	10	71.52
Samavat A [52] (2022)	CNN-BiLSTM	DE	62	84.35
Xu T [53] (2022)	DAGAM	DE	62	92.59
Yuvaraj R [55] (2023)	CART	statistical features,FD,Hjorth, HOS	62	84.49
Proposed method	ACO–CNN–LSTM	DE	**31**	**96.99**

Data Availability Statement

https://bcmi.sjtu.edu.cn/~seed/index.html.

CRediT authorship contribution statement

Xiaodan Zhang: Writing – review & editing, Writing – original draft, Software, Methodology, Funding acquisition. **Kemeng Xu:** Writing – review & editing, Writing – original draft, Software, Methodology. **Lu Zhang:** Writing – original draft, Software. **Rui Zhao:** Methodology, Data curation. **Wei Wei:** Writing – original draft. **Yichong She:** Methodology.

Declaration of competing interest

The authors declare that they have no known competing financial interests or personal relationships that could have appeared to influence the work reported in this paper.

Acknowledgments

This research was funded by National Natural Science Foundation of China, grant number 81901827; Natural Science Basic Research Program of Shaanxi province, grant number 2022JM-146; 2024 Graduate Student Innovation Fund of Xi'an Polytechnic University, grant number chx2024015.

References

[1] Banan Maayah, Abu Arqub Omar, Uncertain M-fractional differential problems: existence, uniqueness, and approximations using Hilbert reproducing technique provisioner with the case application: series resistor-inductor circuit, Phys. Scripta 99 (2) (2024) 025220. https://iopscience.iop.org/article/10.1088/1402-4896/ad1738/meta.
[2] Arqub Abu, Riyane Mezghiche Omar, Banan Maayah, Fuzzy M-fractional integrodifferential models: theoretical existence and uniqueness results, and approximate solutions utilizing the Hilbert reproducing kernel algorithm, Frontiers in Physics 11 (2023) 1252919, https://doi.org/10.3389/fphy.2023.1252919.
[3] M. Dehghani, M. Ghiasi, T. Niknam, et al., Blockchain-based Securing of data Exchange in a Power Transmission system considering Congestion Management and Social Welfare, Sustainability 13 (2021) 90, https://doi.org/10.3390/su13010090.
[4] J. Liu, C. Chen, Z. Liu, et al., An IGDT-based risk-involved optimal bidding strategy for hydrogen storage-based intelligent parking lot of electric vehicles, J. Energy Storage 27 (2020) 101057, https://doi.org/10.1016/j.est.2019.101057.
[5] Z. Yang, M. Ghadamyari, H. Khorramdel, et al., Robust multi-objective optimal design of islanded hybrid system with renewable and diesel sources/stationary and mobile energy storage systems, Renew. Sustain. Energy Rev. 148 (2021) 111295, https://doi.org/10.1016/j.rser.2021.111295.
[6] M. Mehrpooya, N. Ghadimi, M. Marefati, et al., Numerical investigation of a new combined energy system includes parabolic dish solar collector, Stirling engine and thermoelectric device, Int. J. Energy Res. 45 (11) (2021) 16436–16455, https://doi.org/10.1002/er.6891.
[7] B. Chakravarthi, S.C. Ng, M.R. Ezilarasan, et al., EEG-based emotion recognition using hybrid CNN and LSTM classification, Front. Comput. Neurosci. (2022), https://doi.org/10.3389/fncom.2022.1019776.
[8] X. Xing, Z. Li, T. Xu, et al., SAE+ LSTM: a New framework for emotion recognition from multi-channel EEG, Front. Neurorob. 13 (2019) 37, https://doi.org/10.3389/fnbot.2019.00037.
[9] Y. Liu, G. Fu, Emotion recognition by deeply learned multi-channel textual and EEG features, Future Generat. Comput. Syst. 119 (2021) 1–6, https://doi.org/10.1016/j.future.2021.01.010.
[10] H. Ye, G. Jin, W. Fei, et al., High step-up interleaved dc/dc converter with high efficiency, Energy Sources, Part A Recovery, Util. Environ. Eff. (2020) 1–20, https://doi.org/10.1080/15567036.2020.1716111.
[11] R.M. Mehmood, H.J. Yang, S.H. Kim, Children emotion regulation: development of neural marker by investigating human brain signals, IEEE Trans. Instrum. Meas. 70 (2020) 1–11, https://doi.org/10.1109/tim.2020.3011817.
[12] Ozdemir Mehmet Akif, Murside Degirmenci, et al., EEG-based emotion recognition with deep convolutional neural networks, Biomedical Engineering Biomedizinische Tec-hnik 66 (1) (2020) 43–57, https://doi.org/10.13140/RG.2.2.22049.63848.
[13] S. Sheykhivand, Z. Mousavi, T.Y. Rezaii, et al., Recognizing emotions Evoked by Music using CNN-LSTM networks on EEG signals, IEEE Access (99) (2020), https://doi.org/10.1109/access.2020.3011882, 1-1.
[14] W.L. Zheng, B.L. Lu, Investigating Critical frequency bands and channels for EEG-based emotion recognition with deep neural networks, IEEE Transactions on Autonomous Mental Development 7 (3) (2015), https://doi.org/10.1109/tamd.2015.2431497, 1-1.
[15] H. Liu, Y. Zhang, Y. Li, et al., Review on emotion recognition based on electroencephalography, Front. Comput. Neurosci. (2021) 84, https://doi.org/10.1109/tamd.2015.2431497.
[16] K. Kamble, J. Sengupta, A comprehensive survey on emotion recognition based on electroencephalograph (EEG) signals, Multimed. Tool. Appl. (2023) 1–36, https://doi.org/10.1007/s11042-023-14489-9.
[17] F. Yang, X. Zhao, W. Jiang, et al., Cross-subject emotion recognition using multi-method fusion from high-dimensional features, Front. Comput. Neurosci. 13 (2019) 53, https://doi.org/10.3389/fncom.2019.00053.
[18] K.P. Wagh, K. Vasanth, Performance evaluation of multi-channel electroencephalogram signal (EEG) based time frequency analysis for human emotion recognition, Biomed. Signal Process Control 78 (2022) 103966, https://doi.org/10.1016/j.bspc.2022.103966.
[19] M. Ramzan, S. Dawn, Fused CNN-LSTM deep learning emotion recognition model using electroencephalography signals, Int. J. Neurosci. (2021) 1–11, https://doi.org/10.1080/00207454.2021.1941947.
[20] S. Gannouni, K. Belwafi, A. Aledaily, et al., Software Usability testing using EEG-based emotion detection and deep learning, Sensors 23 (11) (2023) 5147, https://doi.org/10.3390/s23115147.
[21] Y. Ji, S.Y. Dong, Deep learning-based self-induced emotion recognition using EEG, Front. Neurosci. (2022) 1589, https://doi.org/10.3389/fnins.2022.985709.
[22] P. Zhong, D. Wang, C. Miao, EEG-based emotion recognition using regularized graph neural networks, IEEE Transactions on Affective Computing (99) (2020).
[23] S.Q. Liu, X. Wang, L. Zhao, et al., Subject-independent emotion recognition of EEG signals based on dynamic empirical convolutional neural network, IEEE ACM Trans. Comput. Biol. Bioinf 18 (5) (2021) 1710–1721, https://doi.org/10.1109/tcbb.2020.3018137.
[24] Y.Q. Yin, X.W. Zheng, B. Hu, et al., EEG emotion recognition using fusion model of graph convolutional neural networks and LSTM, Appl. Soft Comput. 100 (2021) 106954, https://doi.org/10.1016/j.asoc.2020.106954.

[25] Y. Li, W. Zheng, Y. Zong, et al., A Bi-hemisphere domain adversarial neural network model for EEG emotion recognition, IEEE Transactions on Affective Computing (2021), https://doi.org/10.1109/taffc.2018.2885474, 12-2.
[26] G. Bao, B. Yan, L. Tong, et al., Data augmentation for EEG-based emotion recognition using generative adversarial networks, Front. Comput. Neurosci. 15 (2021), https://doi.org/10.3389/fncom.2021.723843.
[27] A. Iyer, S.S. Das, R. Teotia, et al., CNN and LSTM based ensemble learning for human emotion recognition using EEG recordings, Multimed. Tool. Appl. (2022) 1–14, https://doi.org/10.1007/s11042-022-12310-7.
[28] H. He, Y. Tan, J. Ying, et al., Strengthen EEG-based emotion recognition using firefly integrated optimization algorithm, Appl. Soft Comput. 94 (2020) 106426, https://doi.org/10.1016/j.asoc.2020.106426.
[29] N. Razmjooy, F.R. Sheykhahmad, N. Ghadimi, A hybrid neural network–world cup optimization algorithm for melanoma detection, Open Med. 13 (1) (2018) 9–16, https://doi.org/10.1515/med-2018-0002.
[30] A. Parsian, M. Ramezani, N. Ghadimi, A hybrid neural network-gray wolf optimization algorithm for melanoma detection, Biomed Res 28 (8) (2017) 3408–3411. https://api.semanticscholar.org/CorpusID:1050741.
[31] Z. Xu, F.R. Sheykhahmad, N. Ghadimi, et al., Computer-aided diagnosis of skin cancer based on soft computing techniques, Open Med. 15 (1) (2020) 860–871, https://doi.org/10.1515/med-2020-0131.
[32] Z. Gao, Y. Li, Y. Yang, et al., A GPSO-optimized convolutional neural networks for EEG-based emotion recognition, Neurocomputing 380 (2020) 225–235, https://doi.org/10.1016/j.neucom.2019.10.096.
[33] S. Lokesh, T.S. Reddy, An effective optimized deep learning for emotion classification from EEG signals, Signal, Image and Video Processing (2022) 1–12, https://doi.org/10.1007/s11760-022-02373-2.
[34] K. Kannadasan, S. Veerasingam, B. Shameedhabegum, et al., An EEG-based subject-independent emotion recognition model using a differential-evolution-based feature selection algorithm, Knowl. Inf. Syst. (2023), https://doi.org/10.1007/s10115-022-01762-w.
[35] P. Pandey, K.R. Seeja, Subject independent emotion recognition from EEG using VMD and deep learning, Journal of King Saud University-Computer and Information Sciences 34 (5) (2022) 1730–1738, https://doi.org/10.1016/j.jksuci.2019.11.003.
[36] D. Ouyang, Y. Yuan, G. Li, et al., The effect of time Window Length on EEG-based emotion recognition, Sensors 22 (13) (2022) 4939, https://doi.org/10.3390/s22134939.
[37] F. Cui, R. Wang, W. Ding, et al., A novel de-cnn-bilstm multi-fusion model for eeg emotion recognition, Mathematics 10 (4) (2022) 582, https://doi.org/10.3390/math10040582.
[38] W.L. Zheng, J.Y. Zhu, B.L. Lu, Identifying stable patterns over time for emotion recognition from EEG, IEEE Transactions on Affective Computing 10 (3) (2017) 417–429.
[39] M. Tunnicliffe, G. Hunter, Dimensionality, granularity, and differential residual weighted entropy, Entropy 21 (9) (2019) 825, https://doi.org/10.3390/e21090825.
[40] M.K. Shakhatreh, S. Dey, M.T. Alodat, Objective Bayesian analysis for the differential entropy of the Weibull distribution, Appl. Math. Model. 89 (2021) 314–332, https://doi.org/10.1016/j.apm.2020.07.016.
[41] F. Hou, Q. Gao, Y. Song, et al., Deep feature pyramid network for EEG emotion recognition, Measurement 201 (2022) 111724, https://doi.org/10.1016/j.measurement.2022.111724.
[42] X. Lei, H. Pan, X. Huang, A dilated CNN model for image classification, IEEE Access 7 (2019) 124087–124095, https://doi.org/10.1109/access.2019.2927169.
[43] H. Khataei Maragheh, F.S. Gharehchopogh, K. Majidzadeh, et al., A new hybrid based on long short-term memory network with spotted hyena optimization algorithm for multi-label text classification, Mathematics 10 (3) (2022) 488, https://doi.org/10.3390/math10030488.
[44] W.H. Hwang, D.H. Kang, D.H. Kim, Brain lateralisation feature extraction and ant colony optimisation-bidirectional LSTM network model for emotion recognition, IET Signal Process. 16 (1) (2022) 45–61, https://doi.org/10.1049/sil2.12076.
[45] H. Akbari, M.T. Sadiq, A.U. Rehman, et al., Depression recognition based on the reconstruction of phase space of EEG signals and geometrical features, Appl. Acoust. 179 (2021) 108078, https://doi.org/10.1016/j.apacoust.2021.108078.
[46] M. Miao, W. Zhang, W. Hu, et al., An adaptive multi-domain feature joint optimization framework based on composite kernels and ant colony optimization for motor imagery EEG classification, Biomed. Signal Process Control 61 (2020) 101994, https://doi.org/10.1016/j.bspc.2020.101994.
[47] China. SEED dataset. https://bcmi.sjtu.edu.cn/~seed/index.html.
[48] A. Naseer, M. Rani, S. Naz, et al., Refining Parkinson's Neurological Disorder Identification through deep transfer learning, Neural Comput. Appl. 32 (3) (2019) 839–854, https://doi.org/10.1007/s00521-019-04069-0.
[49] T. Song, W. Zheng, P. Song, et al., EEG emotion recognition using dynamical graph convolutional neural networks, IEEE Transactions on Affective Computing (2018), https://doi.org/10.1109/taffc.2018.2817622, 1-1.
[50] Z.M. Wang, Y. Tong, X. Heng, Phase-locking value based graph convolutional neural networks for emotion recognition, IEEE Access 7 (2019) 93711–93722, https://doi.org/10.1109/access.2019.2927768.
[51] S. Hwang, K. Hong, G. Son, H. Byun, Learning cnn features from de features for eeg-based emotion recognition, Pattern Anal Applic 23 (3) (2020) 1323–1335, https://doi.org/10.1007/s10044-019-00860-w.
[52] A. Samavat, E. Khalili, B. Ayati, et al., Deep learning model with adaptive regularization for EEG-based emotion recognition using temporal and frequency features, IEEE Access 10 (2022) 24520–24527, https://doi.org/10.1109/access.2022.3155647.
[53] T. Xu, W. Dang, J. Wang, et al., DAGAM: a domain adversarial graph attention model for subject independent EEG-based emotion recognition, J. Neural. Eng. (2022), https://doi.org/10.1088/1741-2552/acae06.
[54] M.A. Rahman, M.F. Hossain, M. Hossain, et al., Employing PCA and t-statistical approach for feature extraction and classification of emotion from multichannel EEG signal, Egyptian Informatics Journal 21 (1) (2020) 23–35, https://doi.org/10.1016/j.eij.2019.10.002.
[55] R. Yuvaraj, P. Thagavel, J. Thomas, et al., Comprehensive analysis of feature extraction methods for emotion recognition from multichannel EEG recordings, Sensors 23 (2) (2023) 915, https://doi.org/10.3390/s23020915.